Available online at www.sciencedirect.com
SCIENCE DIRECT
Journal of Solid State Chemistry 179 (2006) 1459–1468
JOURNAL OF SOLID STATE CHEMISTRY
www.elsevier.com/locate/jssc

Hydrothermal synthesis, crystal structure, thermal behavior, ferromagnetic resonance and ferrimagnetic behavior of $(C_4H_{12}N_2)_{1.5}[Fe_3(HAsO_4)_{1.02}(HPO_4)_{0.98}(AsO_4)_{0.88}(PO_4)_{0.12}F_5]$

Begoña Bazán[a], José L. Mesa[b,*], José L. Pizarro[a], Luis Lezama[b], A. Peña[b], María I. Arriortua[a], Teófilo Rojo[b,*]

[a]Departamento de Mineralogía y Petrología, Facultad de Ciencia y Tecnología, Universidad del País Vasco, Apdo. 644, E-48080 Bilbao, Spain
[b]Departamento de Química Inorgánica, Facultad de Ciencia y Tecnología, Universidad del País Vasco, Apdo. 644, E-48080 Bilbao, Spain

Received 17 November 2005; received in revised form 27 January 2006; accepted 28 January 2006
Available online 7 March 2006

Abstract

$(C_4H_{12}N_2)_{1.5}[Fe_3(HAsO_4)_{1.02}(HPO_4)_{0.98}(AsO_4)_{0.88}(PO_4)_{0.12}F_5]$ has been synthesized by using mild hydrothermal conditions under autogeneous pressure. The crystal structure was solved from X-ray single crystal data. The compound crystallizes in the monoclinic $P2_1/c$ space group. The unit cell parameters are $a = 8.270(7)$, $b = 22.028(3)$, $c = 10.736(2)$ Å, $\beta = 99.79(2)^\circ$ with $Z = 4$. The crystal structure is formed from $[Fe_3(HAsO_4)_{1.02}(HPO_4)_{0.98}(AsO_4)_{0.88}(PO_4)_{0.12}F_5]^{3-}$ sheets with the piperazinium cations located in the interlayer space, compensating the anionic charge and establishing hydrogen bonds. The IR and Raman spectroscopies confirm the existence of both the arsenate/hydrogenarsenate and phosphate/hydrogenphosphate oxoanions and the presence of the piperazinium dication. The reflectance diffuse spectrum is in good agreement with the existence of iron(III) high spin cations in slightly distorted octahedral geometry. The values of the Dq and Racah parameters are $Dq = 1005$, $B = 1020$ and $C = 2725\,cm^{-1}$. The ESR spectroscopy shows the presence of ferromagnetic resonance. The g-value shifts from 1.99(1) in the 300–15 K range to 3.11(1) at lower temperatures. Magnetic measurements indicate the presence of a ferrimagnetic behavior with the existence of a weak hysteresis loop at 5 K.

Keywords: Hydrothermal synthesis; Crystal structure; Thermal behavior; IR; Raman; UV–visible; ESR; Magnetism

1. Introduction

The world of crystalline porous materials has long been dominated by aluminosilicates zeolites, which are used widely in catalysis, separations, and ion-exchange processes [1]. In the last years, the mild hydrothermal synthesis of organically templated transition metal by using organic diamines as structure-directing agents is a subject of intense research because of their interesting structural chemistry and potential applications [2]. Besides, the addition of fluorhydric acid in the synthesis medium indicates that the fluorine ions act as good mineralizadors leading to new structural types including the fluorine to the inorganic framework [3]. The most important examples were the cloverite [3b] and the ULM-n family ($n<20$) [4].

The incorporation of transition elements to the organically templated open-framework phosphated systems is particularly fascinating due to the possibility of the variation in the coordination environment around the metal ion, as well as, the possibility of observing interesting magnetic properties [5]. In the last years, a large number of transition metal phosphates with open architectures have been synthesized [6]. Among these, a number of works dealing with organically templated iron phosphates, such as those published by Ferey and co-workers have evidenced a rich structural chemistry in this system [5a,5b,6a,7]. Furthermore, open-framework phosphates with paramagnetic cations such as cobalt(II), manganese(II), nickel(II), and vanadium(III,IV) have been also recently synthesized and studied [5c,6c,6d,8,9].

*Corresponding authors. Fax: +34 946013500.
E-mail addresses: qipmeruj@lg.ehu.es (J.L. Mesa), qiproapt@lg.ehu.es (T. Rojo).

0022-4596/$ - see front matter © 2006 Elsevier Inc. All rights reserved.
doi:10.1016/j.jssc.2006.01.073

Arsenates are also interesting anions in comparison with phosphates to be used in the attainment of compounds with occluding organic amines. The synthesis conditions for arsenates are analogous to those for phosphates; however, little work has been carried out on the arsenates compared to the phosphates and in the solid solutions formed by these two oxoanions. To date only several arsenates of gallium(III), molybdenum(IV), vanadium(III), and iron(III) have been reported in the literature [10]. On the other hand, in the solid solution $Li_3Fe_2(AsO_4)_{1-x}(PO_4)_x$ [$x = 0$, 1, 1.5, 2], that exhibits a ferromagnetic behavior, a significant decrease of the Néel temperature with increasing degree of arsenate–phosphate substitution has been observed [11]. This work deals with the synthesis, by using piperazine as template molecule, of $(C_4H_{12}N_2)_{1.5}[Fe_3(HAsO_4)_{1.02}(HPO_4)_{0.98}(AsO_4)_{0.88}(PO_4)_{0.12}F_5]$. The crystal structure of this new mixed anion arsenate–phosphate fluorinated compound is reported. The thermal, spectroscopic and magnetic properties of this phase are discussed.

2. Experimental section

2.1. Synthesis and characterization

$(C_4H_{12}N_2)_{1.5}[Fe_3(HAsO_4)_{0.47}(HPO_4)_{1.53}(AsO_4)_{0.67}(PO_4)_{0.33}F_5]$ (**1**), $(C_4H_{12}N_2)_{1.5}[Fe_3(HAsO_4)_{1.02}(HPO_4)_{0.98}(AsO_4)_{0.88}(PO_4)_{0.12}F_5]$ (**2**), and $(C_4H_{12}N_2)_{1.5}[Fe_3(HAsO_4)_{1.64}(HPO_4)_{0.36}(AsO_4)_{0.97}(PO_4)_{0.03}F_5]$ (**3**) were synthesized by mild-hydrothermal reaction under autogeneous pressure. The starting reagents were $FeCl_3 \cdot 6H_2O$ (0.37 mmol), As_2O_5 [2.775; 1.85; 0.925 mmol for (**1**), (**2**) and (**3**), respectively], $H_3(PO_4)$ [0.925; 1.85 and 0.925 mmol for (**1**), (**2**) and (**3**), respectively], HF (57.5 mmol) and piperazine (8.85 mmol) in ca. 30 mL of water with an initial pH of 1.5. These reaction mixtures were stirred up to homogeneity, sealed in a PTFE-lined stainless steel pressure vessel (fill factor 75%) and heated at 170 °C for 5 days. The pH did not show any appreciable change during the reaction. Prismatic single-crystals with pink color were obtained in all cases, which were filtered off, washed with water and acetone, and dried over P_2O_5 for 2 h. Additionally, they were synthesized, using the same procedure, two phases, in which the crystal structure was not resolved from single-crystal X-ray diffraction data, and corresponds to the $(C_4H_{12}N_2)_{1.5}[Fe_3(HAsO_4)_{2-x}(HPO_4)_x(AsO_4)_{1-y}(PO_4)_yF_5]$ general formula with an As:P ratio of 35:65 and 15:85.

The $(C_4H_{12}N_2)_{1.5}[Fe_3(HPO_4)_2(PO_4)F_5]$ (**4**) compound cannot be obtained using similar chemical conditions to those applied to obtain the mixed arsenate–phosphate compounds. So, these synthesized phases form a finite solid solution in which the higher limit is, approximately, 50%/60% of phosphate/hydrogenphosphate oxoanions.

Chemical analysis by inductively coupled plasma atomic emission spectroscopy (ICP-AES), performed with an ARL Fisons 3410 spectrometer, was used to confirm the amount of the iron, arsenic, and phosphorus elements. C, H, N-elemental analysis was carried out with a Perkin–Elmer Model 240 automatic analyzer. Fluorine content was determined by using a selective electrode. Found: Fe, 22.3; As, 11.4; P, 7.6; C, 9.6; N, 5.4; H, 3.7; F, 12.5. $(C_4H_{12}N_2)_{1.5}[Fe_3(HAsO_4)_{0.47}(HPO_4)_{1.53}(AsO_4)_{0.67}(PO_4)_{0.33}F_5]$ (**1**) requires Fe, 22.6; As, 11.5; P, 7.8; C, 9.7; N, 5.7; H, 3.9; F, 12.8. Found: Fe, 23.9; As, 20.2; P, 4.1; C, 10.0; N, 5.7; H, 2.6; F, 13.1. $(C_4H_{12}N_2)_{1.5}[Fe_3(HAsO_4)_{1.02}(HPO_4)_{0.98}(AsO_4)_{0.88}(PO_4)_{0.12}F_5]$ (**2**) requires Fe, 24.4; As, 20.8; P, 4.9; C, 10.5; N, 6.1; H, 2.9; F, 13.8. Found: Fe, 20.5; As, 24.1; P, 1.3; C, 8.6; N, 5.1; H, 3.4; F, 11.6. $(C_4H_{12}N_2)_{1.5}[Fe_3(HAsO_4)_{1.64}(HPO_4)_{0.36}(AsO_4)_{0.97}(PO_4)_{0.03}F_5]$ (**3**) requires Fe, 20.8; As, 24.3; P, 1.5; C, 8.9; N, 5.2; H, 3.6; F, 11.8. The densities, measured by flotation in a mixture of $CHBr_3/CHCl_3$, are 2.19(1), 2.32(2) and 2.50(2) g cm^{-3}, for (**1**), (**2**) and (**3**), respectively.

The X-ray powder diffraction patterns of these compounds are shown in Fig. 1. They are in good agreement with the calculated diffractograms based on the results from single-crystal X-ray diffraction, indicating the existence of isoestructurality and pure phases with high crystallinity.

2.2. Crystal structure resolution of $(C_4H_{12}N_2)_{1.5}[Fe_3(HAsO_4)_{1.02}(HPO_4)_{0.98}(AsO_4)_{0.88}(PO_4)_{0.12}F_5]$

A suitable single-crystal for (**2**) with dimensions $0.2 \times 0.1 \times 0.1$ was carefully selected under a polarizing microscope and mounted on a glass fiber. Intensities of the diffraction data were measured at room temperature on an Enraf-Nonius CAD4 automated diffractometer, using graphite-monochromatized Mo$K\alpha$ radiation. An Oxford Diffraction XCALIBUR automated diffractometer was used to collect the intensity data for (**1**) and (**3**) phases. Crystallographic data for phase (**2**) are reported in Table 1. Table 2 gives the unit-cell parameters obtained from the structural resolution of the compounds (**1**), (**2**), (**3**) and (**4**).

A total of 4628 reflections were measured for (**2**) in the $1.85° \leqslant \theta \leqslant 27.48°$ range. A total of 4400 reflections were independent ($R_{int.} = 0.028$) and 3259 observed applying the criterion $I > 2\sigma(I)$. Correction for Lorentz and polarization effects were done and also for absorption with the empirical ψ scan method [12] by using the X-RAYACS program [13]. Direct methods (SHELXS 97) [14] were employed to solve the structure and refined by the full-matrix least-squares procedure based on F^2, using the SHELXL 97 computer program [15] belonging to the WINGX software package [16]. The scattering factors were taken from Ref. [17]. The atomic coordinates and the temperature factors of the arsenic and phosphorus atoms belonging to the arsenate/hydrogen-arsenate and phosphate/hydrogen-phosphate anions in phase (**2**), respectively, were refined together, and their occupancy factors were constricted to sum one. The final occupancy factors were 0.88/0.12, 0.38/0.62 and 0.64/0.36 for the As(1)/P(1)O_4, HOAs(2)/P(2)O_3 and HOAs(3)/P(3)O_3 tetrahedra, respectively. In phase (**1**), the final refined occupancy

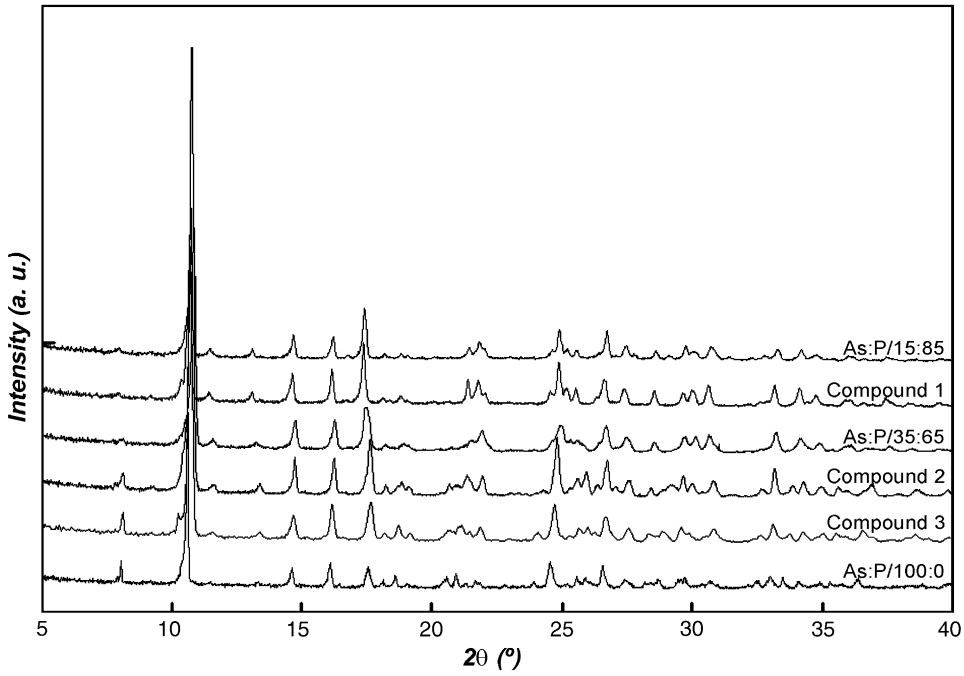

Fig. 1. X-ray powder diffraction patterns of the synthesized compounds.

Table 1
Crystallographic data and details of the crystal structure refinement

Chemical formula	$(C_4H_{12}N_2)_{1.5}[Fe_3(HAs_{0.51}P_{0.49}O_4)_2(As_{0.88}P_{0.12}O_4)F_5]$
Formula weight ($g\,mol^{-1}$)	765.18
a, Å	8.270(7)
b, Å	22.028(3)
c, Å	10.736(2)
β, deg.	99.79(2)
V, Å^3	1927.3(2)
Z	4
Space group	$P2_1/c$ (no. 14)
T, °C	293(2)
Radiation, λ(Mo$K\alpha$), Å	0.71073
$\rho_{obsd.}$, $\rho_{calcd.}$, $g\,cm^{-3}$	2.32(2), 2.364
μ (Mo$K\alpha$), mm^{-1}	4.747
R [$I > 2\sigma(I)$]	$R_1 = 0.033$ w$R_2 = 0.068$
R [all data]	$R_1 = 0.072$ w$R_2 = 0.076$
GOF	1.028

$R_1 = [\Sigma(|F_o| - |F_c|)]/\Sigma|F_o|$; w$R_2 = [\Sigma[w(|F_o|^2 - |F_c|^2)^2]/\Sigma[w(|F_o|^2)^2]]^{1/2}$; $w = 1/[\sigma^2|F_o|^2 + (xp)^2 + yp]$; where $p = [|F_o|^2 + 2|F_c|^2]/3$; $x = 0.0315$, $y = 1.7027$.

Table 2
Unit-cell parameters obtained from single-crystal X-ray diffraction resolution for compounds (**1**), (**2**), (**3**) and for $(C_4H_{12}N_2)_{1.5}[Fe_3(HAsO_4)_2(AsO_4)F_5]$ (**4**)

Compound	(**1**)	(**2**)	(**3**)	(**4**)
a (Å)	8.330(1)	8.270(7)	8.397(2)	8.357(1)
b (Å)	22.106(3)	22.028(3)	22.146(4)	21.942(6)
c (Å)	10.707(2)	10.736(2)	10.870(2)	10.828(3)
β (deg.)	99.54(1)	99.79(2)	96.63(2)	96.24(2)

factors are 0.67/0.33, 0.15/0.85 and 0.33/0.67 for the As(1)/P(1)O_4, HOAs(2)/P(2)O_3 and HOAs(3)/P(3)O_3 tetrahedra, respectively. For phase (**3**) the final occupancy factors are 0.97/0.03, 0.79/0.21 and 0.86/0.14 for As(1)/P(1)O_4, HOAs(2)/P(2)O_3 and HOAs(3)/P(3)O_3 tetrahedra, respectively. All non-hydrogen atoms of compound (**2**) were assigned anisotropic thermal parameters. The hydrogen atoms of the hydrogen-arsenate/phosphate anions were obtained from the Fourier maps and those of the piperazinium dication were geometrically placed. For (**2**), the final R factors (all data) were $R_1 = 0.072$ [w$R_2 = 0.076$]. Maximum and minimum peaks for (**2**) in final difference synthesis were 0.716, $-0.808\,eÅ^{-3}$. The final atomic coordinates and thermal parameters have been deposited at the Cambridge Crystallographic Data Centre (CCDC 212102). The drawings of the crystal structure were performed using ATOMS program [18]. Selected bond distances for (**2**) are listed in Table 3.

2.3. Physical measurements

The IR spectrum (KBr pellets) was obtained with a Nicolet FT-IR 740 spectrophotometer in the 400–4000 cm^{-1} range. The Raman spectrum was recordered in the 200–3000 cm^{-1} range, with a Nicolet 950FT spectrophotometer equipped with a neodymium laser emitting at 1064 nm. The diffuse reflectance spectrum was registered at room temperature on a Cary 2415 spectrometer in the 210–2000 nm range. A Bruker ESP 300 spectrometer was used to record the EPR polycrystalline spectra from room temperature to 4.2 K. The temperature was stabilized by an Oxford Instrument (ITC 4) regulator. The magnetic field

Table 3
Selected bond distances (Å) (e.s.d. in parentheses)

Fe(1)O$_4$F$_2$ octahedron		*Fe(2)O$_3$F$_3$ octahedron*		*Fe(3)O$_3$F$_3$ octahedron*	
Fe(1)–O(7)	1.955(3)	Fe(2)–F(3)	1.928(3)	Fe(3)–F(5)	1.867(3)
Fe(1)–O(4)	1.976(3)	Fe(2)–O(1)^{ii}	1.937(3)	Fe(3)–O(9)^{ii}	1.925(3)
Fe(1)–F(2)	1.986(3)	Fe(2)–O(11)	1.953(3)	Fe(3)–O(3)	1.961(3)
Fe(1)–O(5)^{i}	1.991(3)	Fe(2)–O(6)	1.974(3)	Fe(3)–F(4)^{iii}	2.010(2)
Fe(1)–O(10)	2.008(3)	Fe(2)–F(2)^{ii}	1.993(2)	Fe(3)–O(2)^{iii}	2.020(3)
Fe(1)–F(1)	2.011(2)	Fe(2)–F(1)	2.041(2)	Fe(3)–F(4)	2.073(3)
As/P(1)O$_4$ tetrahedron		*HOAs/P(2)O$_3$ tetrahedron*		*HOAs/P(3)O$_3$ tetrahedron*	
As/P(1)–O(4)	1.660(3)	As/P(2)–O(6)	1.572(3)	As/P(3)–O(10)	1.622(3)
As/P(1)–O(1)	1.668(3)	As/P(2)–O(7)	1.584(3)	As/P(3)–O(11)	1.636(3)
As/P(1)–O(2)	1.675(3)	As/P(2)–O(5)	1.587(3)	As/P(3)–O(9)	1.641(3)
As/P(1)–O(3)	1.681(3)	As/P(2)–O(8)	1.609(3)	As/P(3)–O(12)	1.683(3)
(C$_4$H$_{12}$N$_2$)$^{2+}$					
N(1)–C(3)	1.486(7)	N(1)–C(2)	1.499(7)	N(2)–C(4)	1.487(6)
N(2)–C(1)	1.495(6)	N(3)–C(5)	1.477(8)	N(3)–C(6)	1.523(8)
C(1)–C(2)	1.499(7)	C(3)–C(4)	1.508(7)	C(5)–C(6)^{iv}	1.466(7)
C(6)–C(5)^{iv}	1.466(7)				

Symmetry codes: i = $x, -y+3/2, z-1/2$; ii = $x, -y+3/2, z+1/2$; iii = $-x+1, -y+1, -z+1$; iv = $-x, -y+1, -z$.

was measured with a Bruker BNM 200 gaussmeter and the frequency inside the cavity was determined using a Hewlett-Packard 5352B microwave frequency counter. Magnetic measurements on powdered sample were performed in the temperature range 5.0–300 K, using a Quantum Design MPMS-7 SQUID magnetometer. The magnetic field was 1000 Oe, a value in the range of linear dependence of magnetization vs. magnetic field, even at 5.0 K.

3. Results and discussion

3.1. Thermal study

The thermal decomposition curve reveals, between 250 and 350 °C, a continuous weight loss of approximately 29.0. This result can be attributed to the simultaneous loss of the piperazinium dication and the fluorine ions present in the compound (calc. 29.7). After this process a weight loss of approximately 5% occurs in the 350–500 °C range. This loss suggests the existence of condensation of the hydrogen-arsenate/phosphate oxoanions, and a partial decomposition of these oxoanions, together with a sublimation process, giving rise to As_2O_3 and/or As_2O_5/P_2O_5 [10e]. The X-ray diffraction patterns of the residues obtained from the thermogravimetric analysis at 800 °C show the presence of peaks which can be attributed to the Fe(AsO_4) [$P2_1/n$ with $a = 5.01(1)$, $b = 8.08(1)$, $c = 7.57(1)$ Å and $\beta = 104.5(1)°$] [19a] and Fe(PO_4) [$P3_121$ with $a = b = 5.03(1)$, $c = 11.23(1)$ Å] [19b] phases.

The thermal behavior was also studied by using time-resolved X-ray thermodiffractometry in air atmosphere. A PHILIPS X'PERT automatic diffractometer (Cu$K\alpha$ radiation) equipped with a variable-temperature stage (Paar Physica TCU2000) with a Pt sample holder was used in the experiment. The powder patterns were recorded in 2θ steps of 0.02° in the $5 \leqslant 2\theta \leqslant 45°$ range, counting for 1s per step and increasing the temperature at 5 °C min^{-1} from room temperature up to 800 °C. The results are given in Fig. 2. The compound is stable up to approximately 300 °C, and the intensity of the monitored (100) peak at $2\theta = 10.8$, remains practically unchanged. After this temperature the decomposition of the compound gives rise to an amorphous phase between 300 and 540 °C. This result indicates the collapse of the crystal structure with the calcination of the organic cation and the loss of the fluoride anions. The thermodiffractograms performed above 540 °C show the peaks corresponding to Fe(PO_4) [19b]. From 690 to 800 °C the simultaneous presence of Fe(PO_4) [19b] and Fe(AsO_4) is observed [19a]. In the case of the related $(C_4H_{12}N_2)_{1.5}[Fe_3(HAsO_4)_2(AsO_4)F_5]$ phase [20] diffraction peaks appear in the range 525–595 °C, corresponding to a new trigonal Fe(AsO_4) phase, which is isostructural with Fe(PO_4) [21]. The unit-cell parameters of this new polymorph of Fe(AsO_4) have been determined from the Rietveld analysis by using the structural model of the trigonal Fe(PO_4) [20] phase and the FULPROOF program [22]. The refined parameters are $a = b = 5.122(4)$, $c = 11.535(1)$, $V = 262.1$ Å^3 and $Z = 3$, with the $P3_121$ space group.

3.2. Structural description

$(C_4H_{12}N_2)_{1.5}[Fe_3(HAsO_4)_{1.02}(HPO_4)_{0.98}(AsO_4)_{0.88}(PO_4)_{0.12}F_5]$ shows a layered structure constructed from $[Fe_3(HAsO_4)_{1.02}(HPO_4)_{0.98}(AsO_4)_{0.88}(PO_4)_{0.12}F_5]^{3-}$ inorganic sheets extended in the (100) plane (Fig. 3a). The piperazinium dications are located in the interlayer space. The anionic charge of the inorganic skeleton is compensated by the

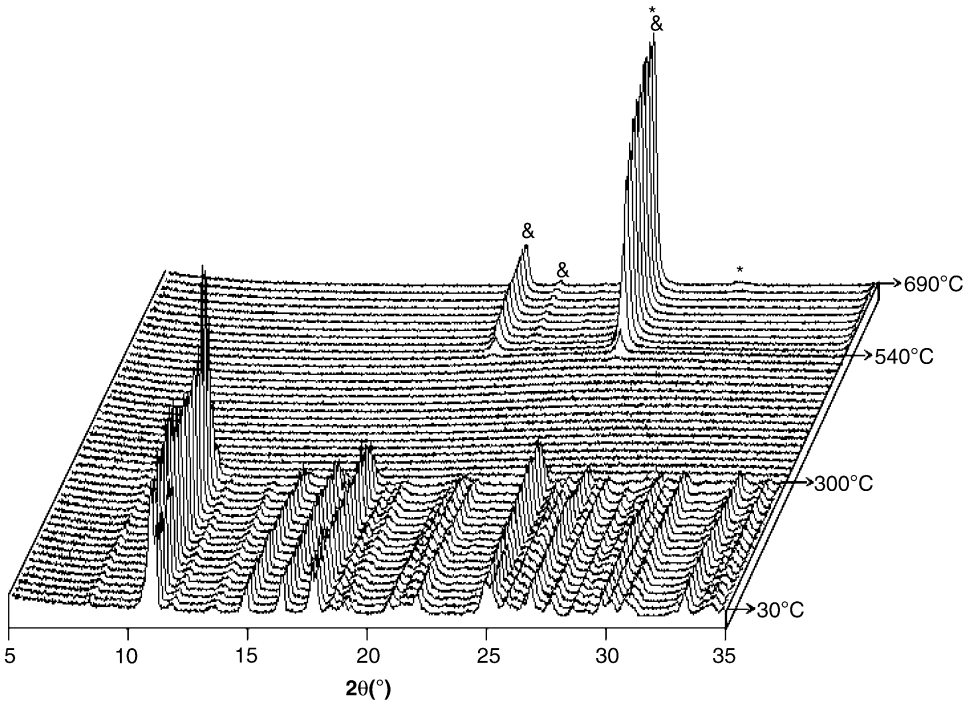

Fig. 2. Thermodiffractogram showing the peaks of the $Fe(PO_4)^{\&}$, and $Fe(AsO_4)^{*}$ phases.

organic dications, which also establish hydrogen bonds with the inorganic fragment.

The layers are formed from chains built by vertex-sharing $Fe(1)O_4F_2$ and $Fe(2)O_3F_3$ octahedra, running along the *c*-axis, and the edge-sharing $Fe(3)_2O_6F_4$ dimeric entities (Fig. 3b). The chains and the $Fe(3)_2O_6F_4$ dimmeric units are connected through the $X(1)O_4$-arsenate/phosphate and $HOX(3)O_3$-hydrogenarsenate/phosphate anions. Two types of cavities can be distinguished in the structure: (i) Cavities of six-members delimited by one $Fe(2)O_3F_3$ and two $Fe(1)O_4F_2$ octahedra, belonging to the chains, which are linked through the $X(1)O_4$ and $HOX(3)O_3$ groups to the $Fe(3)O_3F_3$ octahedron from the $Fe(3)_2O_6F_4$ dimers; (ii) Cavities of eight-members formed by two $Fe(2)O_3F_3$ and two $Fe(3)O_3F_3$ octahedra linked in alternate way by the $X(1)O_4$ and $HOX(3)O_3$ anions. The piperazinium dications are located inside of both types of cavities, which gives rise to channels in the [100] direction by stacking of the layers.

In the chains, the Fe(1) cation from the $Fe(1)O_4F_2$ octahedra is bonded to the $X(1)O_4$, $HOX(2)O_3$ and $HOX(3)O_3$ groups, through the O(4), O(7)–$O(5)^{i}$ and O(10) oxygen atoms with mean length of 1.98(2) Å. The coordination sphere is completed by the F(1) and F(2) fluoride ions, bonded at a mean distance of 2.00(1) Å. The coordination around the Fe(2) cation belonging to the $Fe(2)O_3F_3$ octahedra is established by the $O(1)^{ii}$, O(6) and O(11) atoms, from the $X(1)O_4$, $HOX(2)O_3$ and $HOX(3)O_3$ anions, with a mean distance of 1.96(2) Å. The F(1), $F(2)^{ii}$ and F(3) ions exhibit mean bond length with the Fe(2) cations of 1.99(5) Å. The *cis*-O/F–Fe(1)/Fe(2)–O/F angles are in the 86.3(1)–95.7(1)° and 82.3(1)–97.5(1)° range, respectively, whereas the *trans*-O/F–Fe(1)/Fe(2)–O/F angles deviate from the ideal value by approximately 5°. The distortion of these polyhedra, from an octahedron ($\Delta = 0$) to a trigonal prism ($\Delta = 1$), calculated by quantification of the Muetterties and Guggenberger description [23] is $\Delta = 0.012$ and 0.013 for the octahedra belonging to the Fe(1) and Fe(2) cations, respectively. These values indicate a topology near to octahedron.

In the $Fe(3)O_3F_3$ octahedra from the dimmers, the Fe(3) ions are bonded to the $O(2)^{iii}$ and O(3) from the $X(1)O_4$ arsenate/phosphate and to the $O(9)^{ii}$ atom from the $HOX(3)O_3$ hydrogen-arsenate/phosphate, with mean bond length of 1.97(4) Å. The F(4), $F(4)^{iii}$ and F(5) ions complete the coordination sphere of this cation with a mean distance of 1.98(9) Å. The *cis*-O/F–Fe(3)–O/F angles range from 83.7(1) to 94.2(1)°, and the *trans*-O/F–Fe(2)–O/F angles deviate approximately 9° from the ideal value. The distortion of this polyhedron, from an octahedron ($\Delta = 0$) to a trigonal prism ($\Delta = 1$), is $\Delta = 0.031$, greater than those corresponding to the $Fe(1)O_4F_2$ and $Fe(2)O_3F_3$ polyhedra, and indicates an octahedral geometry [23].

The arsenic and phosphorus atoms adopt tetrahedral coordination. The mean value of the As/P–O bond lengths in the $As(1)_{0.88}P(1)_{0.12}O_4$ arsenate/phosphate anions is 1.671(9) Å. This bond distance is slightly higher than that found for the H–O(8)–$As(2)_{0.38}P(2)_{0.62}O_3$ and H–O(12)–$As(3)_{0.64}P(3)_{0.36}O_3$ hydrogen-arsenate/phosphate anions of 1.59(1) and 1.65(2) Å, respectively, as corresponds to a higher amount of arsenate anion in the $X(1)O_4$ groups. The

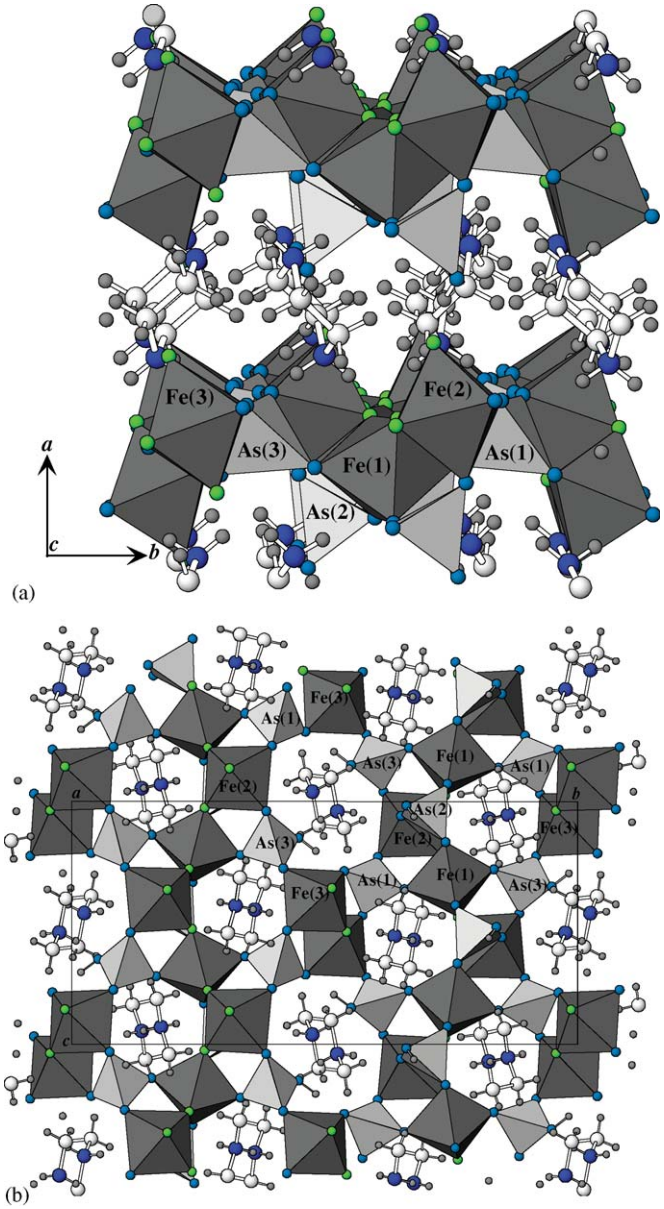

Fig. 3. (a) Polyhedral view of the layered crystal structure. (b) Polyhedral representation of a layer.

O–As/P–O angles in these oxoanions are near to the ideal value expected for a sp^3 hybridization of the central atom in the arsenate and phosphate anions. The mean bond lengths of the XO_4 and $HOXO_3$ tetrahedra of the arsenate/phosphate and arsenate phases follow a linear relation with respect to the amount of arsenic or phosphorus present in these oxoanions (see Fig. 4) indicating that the substitution of arsenic by phosphate has taken place for all the phases.

The bond distances and angles in the piperazinium dication are in the range habitually found for this molecule [21]. The H–O(8)–$As(2)_{0.38}P(2)_{0.62}O_3$ and H–O(12)–$As(3)_{0.64}P(3)_{0.36}O_3$ hydrogen-arsenate/phosphate anions establish hydrogen bonds with F(3) and O(2) atoms belonging to the $Fe(2)O_3F_3$ and $Fe(3)O_3F_3$ octahedra at 2.481(1) Å and 2.698(1) Å, respectively. Moreover, the organic cation forms mono-, bi- and tri-furcated hydrogen bonds through the nitrogen atoms with the fluorine and oxygen coordinated to the metallic ions. The hydrogen bond distances are N(3)–H(13N)···O(11), 2.48(1) Å; N(2)H(22N)···O(3),O(9), 1.89(1), 2.57(1) Å, and N(2)–H(12N)···F(1),F(2),F(3), 2.05(1), 2.49(1), 2.53(1) Å.

The layers show values for the Fe(1)–F(1)–Fe(2) and Fe(1)–F(2)–$Fe(2)^{i}$ angles along the chains of 133.4(1)°, 130.9(1)°. In the $Fe(3)_2O_6F_4$ dimeric entities the $Fe(3)^{iii}$–F(4)–Fe(3) angle is 101.0(1)°. The connection between the Fe(1), Fe(2) and Fe(3) metallic cations with the arsenate-hydrogenarsenate and phosphate-hydrogenphosphate anions along the chains and the dimeric entities takes place via oxygen atoms with *X*–O–*M* angles ranging from 125.1(2) to 140.9(2)°.

3.3. IR, Raman and UV–visible spectroscopies

The results of the IR and Raman spectra and the assignment of bands are given in Table 4. The more characteristic bands corresponding to the vibrations of the piperazinium cation, arsenate/phosphate and hydrogenarsenate/phosphate oxoanions are observed in the spectra. The positions of these bands are similar to those observed for other related arsenate and phosphate compounds [5c,10g,10h,10i,24].

The diffuse reflectance spectrum exhibits bands at 13 820, 18 880, 23 860 and 26 930 cm^{-1}. The intensity of these bands is weak as expected for the spin forbidden transitions between the ground state $^6A_{1g}(^6S)$ and the excited levels $^4T_{1g}(^4G)$; $^4T_{2g}(^4G)$; $^4A_{1g}(^4G)$, $^4E_g(^4G)$ and $^4T_{2g}(^4D)$ of a d^5-high spin cation in regular octahedral symmetry [25]. The *Dq* and Racah (*B* and *C*) parameters were calculated by using the energy expressions for an iron(III) high spin cation in octahedral geometry. The values obtained are $Dq = 1005\,cm^{-1}$, $B = 1020\,cm^{-1}$ and $C = 2725\,cm^{-1}$. These results are in the range habitually found for the iron(III) cation in a slightly distorted octahedral environment [25]. The reduction of the *B*-parameter value respect to that of the free ion ($1150\,cm^{-1}$) is approximately 89%, suggesting a covalent character of the Fe–O, F chemical bonds.

3.4. ESR and magnetic properties

The ESR spectra have been recorded on powdered sample at X-band between 4.2 and 300 K (Fig. 5).

The spectra remain unchanged upon cooling the sample from room temperature to approximately 90 K. Below this temperature the linewidth of the spectrum broadens up to approximately 45 K. When the sample is additionally cooled the linewidth of the spectrum narrows and its intensity increases vigorously. The isotropic signals observed in the 290–15 K range change their line-shape below 10 K and the resonance becomes less symmetrical. The resonances at 10 and 4 K are centered at 243.5 and

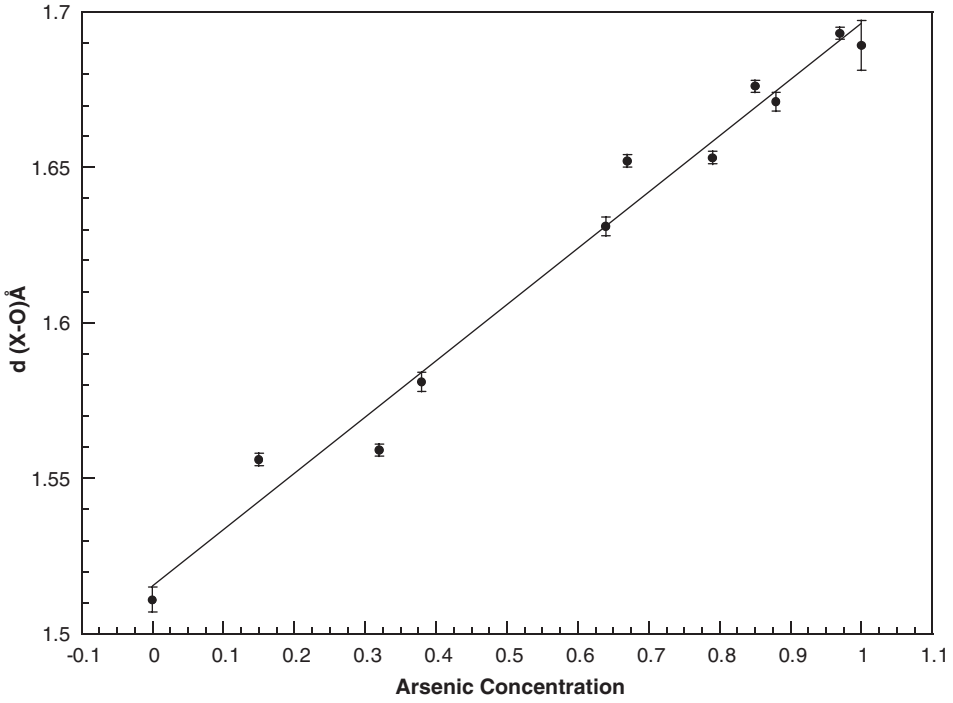

Fig. 4. Representation of the mean bond distances inside the XO_4 tetrahedra vs. arsenic concentration.

Table 4
Selected bands (values in cm^{-1}) from the IR and Raman spectra

Assignment	IR	Raman
ν $(-NH_2)^+$	3140 (s)	3020 (m)
ν $(-CH_2-)$	2920–2600 (w)	2980–2900 (w)
δ $(-NH_2)^+$	1590 (m)	1595 (w)
δ $(-CH_2-)$	1400–1200 (w)	1500–1400 (m)
ν_{as} (PO_4)	1110,1050,1025 (s)	1095,1040,1010 (w)
ν_s (PO_4)	995 (m)	995 (w)
δ_{as} (PO_4)	620,580 (m)	620,610 (w)
ν_{as} (AsO_4)	905,865,800 (s)	880,845,810 (s)
ν_s (AsO_4)	745 (m)	745 (w)
δ_{as} (AsO_4)	500,445 (m)	530,440 (m)
δ (HOAs)	1230 (w)	1045 (m)
δ (HOP)	1475 (w)	1390 (s)

ν = stretching, δ = deformation, s = symmetric, as = asymmetric, s = strong, m = medium, w = weak.

215.8 mT, respectively, with g-values of 2.73(1) and 3.11(1), as a consequence of the higher internal field that shifts the signal from its usual value of 1.99(1) as expected for an iron(III) cation octahedrically coordinated. These features are probably due to a ferromagnetic resonance phenomenon, as was observed in other similar systems [26].

The thermal variations of the intensity and the linewidth of the signals have been calculated by fitting the experimental spectra to Lorentzian curves (Fig. 6).

The intensity increases slightly from room temperature to approximately 50 K. Below this temperature the intensity of the signals increases vigorously. The linewidth of the ESR signals slightly increases in the 300–100 K temperature range, as a consequence of the dipolar homogeneous broadening [27]. When the temperature is further decreased the linewidth increases vigorously due to a strong spin correlation [27], and reaches a maximum at approximately 40 K. From this temperature up to approximately 20 K the linewidth of the signals narrows, and they broaden again below this temperature. This later broadening is probably due to an effect of integration of the signals, caused by the large linewidth of the curves at low temperatures. The narrowing of the ESR signals, the strong increase of their intensities and the large displacement of the g-tensor from its usual value of 2.0 for the iron(III) cation, observed in this compound in the 40–15 K range, can be related to the existence in the phases of a ferromagnetic resonance phenomenon as described before.

Variable-temperature magnetic susceptibility measurements were performed on a powdered sample in the 300–5.0 K temperature range. Fig. 7 shows the thermal evolution of the χ_m vs. T curve. χ_m increases from room temperature with decreasing temperature and reaches a maximum at 8.5 K, indicating that a magnetic ordering is established at this temperature. After that, the susceptibility slightly decreases until 5 K. The thermal evolution of χ_m follows the Curie–Weiss law at temperatures higher than 100 K, with $C_m = 13.52\,cm^3\,K/mol$ and $\theta = -95.8$ K. Moreover, the $\chi_m T$ vs. T product (see Fig. 7) decreases from $10.50\,cm^3\,K/mol$ at room temperature up to

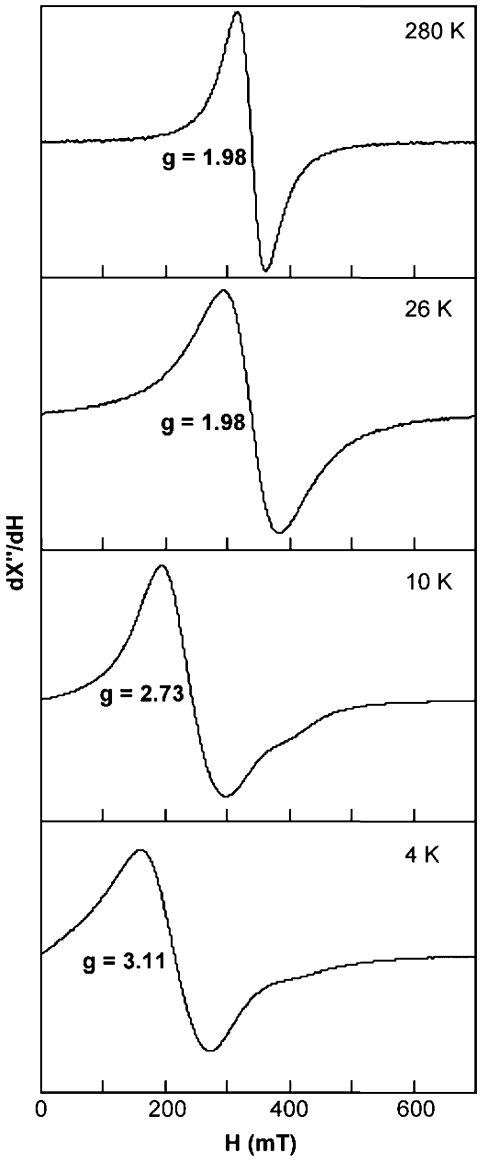

Fig. 5. Powder X-band ESR spectra at different temperatures.

4.90 cm^3K/mol at 40.0 K. However, at lower temperatures an abrupt increase is observed with a maximum at 13.4 K. After this temperature the $\chi_m T$ curve again decreases up to 5 K. These results indicate the existence of a ferrimagnetic behavior, which can take place due to the incomplete compensation of the magnetic moments of the $Fe(1)O_4F_2$, $Fe(2)O_3F_3$ and $Fe(3)O_3F_3$ sublattices.

In order to study the ferromagnetic contributions magnetization measurements were carried out. The variation of the magnetization with the magnetic field at 5 K shows a small hysteresis loop in which the values of the coercive field and remanent magnetization are, approximately, 16 Oe and 55 emu/mol, respectively (see inset in Fig. 8). Furthermore, as can be seen in Fig. 6 the magnetization curve practically reaches the saturation at, approximately, 26 000 emu/mol at 6 T. This value corresponds to 4.65 electrons, close to the five electrons corresponding to a high spin iron(III) cation completely magnetized. These results confirm the existence of a ferromagnetic contribution intrinsic to the sample [28].

4. Concluding remarks

The crystal structure of the mixed arsenate/phosphate phase, solved by X-ray single crystal data, reveals a layered structure. The characterization by IR spectroscopy shows the simultaneous existence of the arsenate/hydrogenarsenate and phosphate/hydrogenphosphate anions. The *Dq*, *B* and *C* parameters are characteristic of high spin iron(III) cations. The ESR spectra indicate the presence of ferromagnetic resonance. The isotropic spectra become less symmetrical at low temperatures. The *g*-value move from the 1.99(1) usual value for an iron(III) octahedrically coordinated cation into greater values. Magnetic measurements are consistent with a ferrimagnetic behavior. The small hysteresis loop shows a value of 16 Oe for the coercive field, whereas the remanent magnetizations is of 55 emul/mol.

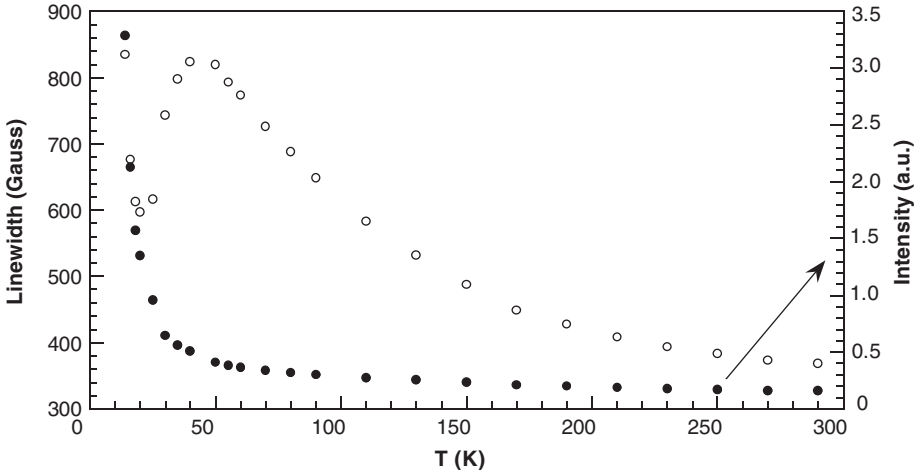

Fig. 6. Temperature dependence of the intensity of the signal and the linewidth curves.

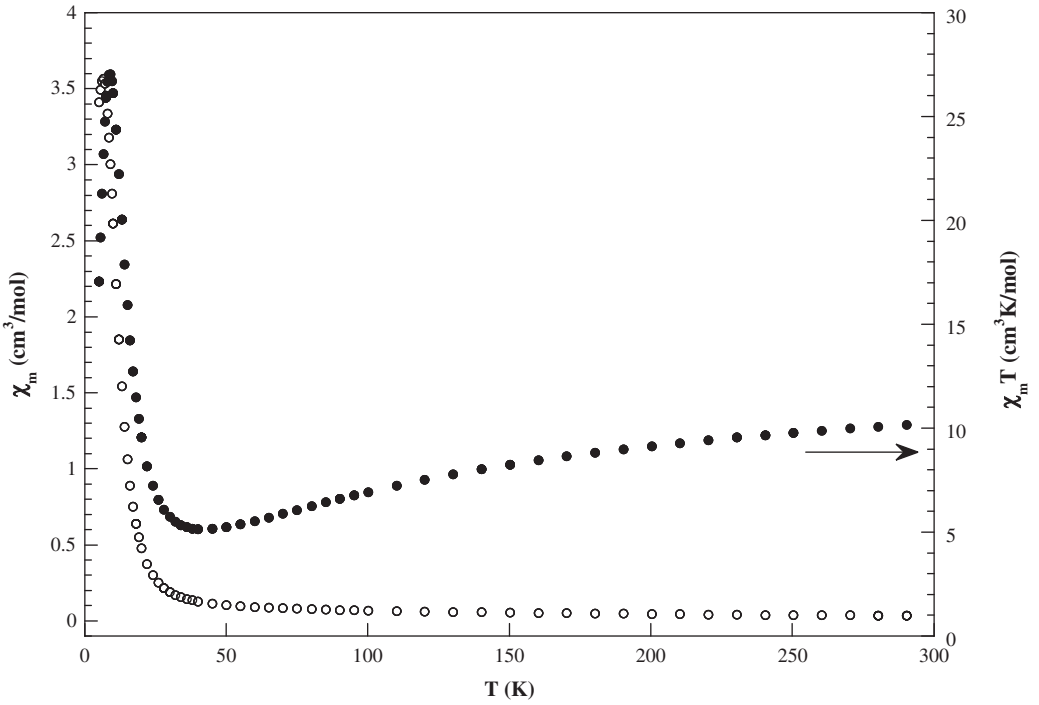

Fig. 7. Thermal evolution of the χ_m and $\chi_m T$ vs. T curves.

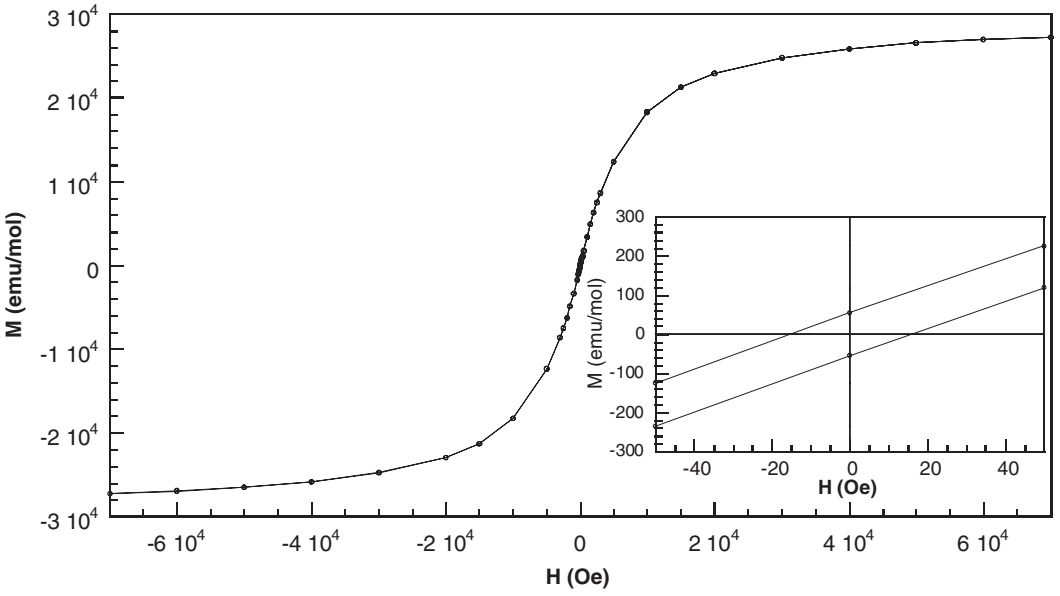

Fig. 8. Hysteresis loop at 5 K.

Acknowledgments

This work was financially supported by the "Ministerio de Educación y Ciencia" (MAT-2004-02071), the "Universidad del País Vasco" (UPV/EHU) (9/UPV00130.310-15967/2004; 9/UPV00169.310-13494/2001) which we gratefully acknowledge. The authors thank the technician of SGIker, Dr. J.P. Chapman financed by the "National Program for the Promotion of Human Resources within the National Plan of Scientific Research, Development and Innovation", "Ministerio de Ciencia y Tecnonolgia" and "Fondo Social Europeo (FSE)", for the X-ray diffraction measurements B. Bazan wishes to thank the Universidad del País Vasco/EHU for funding.

Appendix A. Supplementary materials

Supplementary data associated with this article can be found in the online version at doi:10.1016/j.jssc.2006.01.073.

References

[1] M.E. Davis, Chem. Eur. J. 3 (1997) 1745.
[2] (a) S.T. Wilson, B.M. Lok, C.A. Messina, T.R. Cannan, E.M. Flanigen, J. Am. Chem. Soc. 104 (1982) 1146;
(b) M. Riou-Cavellec, D. Riou, G. Férey, Inorg. Chim. Acta 291 (1999) 317.
[3] (a) J.L. Guth, H. Kessler, R. Wey, Stud. Sci. Catal. 28 (1986) 121;
(b) M. Riou-Cavellec, J.M. Greneche, D. Riou, G. Ferey, Chem. Mater. 10 (1998) 2434.
[4] (a) M. Estermann, L.B. McCusker, C. Baerlocher, A. Merrouche, H. Kessler, Nature 352 (1991) 320;
(b) T. Loisseau, Ph.D. Thesis, Université du Maine (Le Mans), France, 1994.
[5] (a) J.R.D. DeBord, W.M. Reiff, C.J. Warren, R. Haushalter, J. Zubieta, Chem. Mater. 9 (1997) 1994;
(b) J.R.D. DeBord, W.M. Reiff, R.C. Haushalter, J. Zubieta, J. Solid State Chem. 125 (1996) 186;
(c) J. Escobal, J.L. Pizarro, J.L. Mesa, L. Lezama, R. Olazcuaga, M.I. Arriortua, T. Rojo, Chem. Mater. 12 (2000) 376.
[6] (a) K.H. Lii, Y.F. Huang, V. Zima, C.Y. Huang, H.M. Lin, Y.C. Jiang, F.L. Liao, S.L. Wang, Chem. Mater. 10 (1998) 2599;
(b) P. Feng, X. Bu, G.D. Stucky, Nature 388 (1997) 735;
(c) N. Guillou, Q. Gao, M. Nogues, R.E. Morris, M. Hervieu, G. Ferey, A.K. Cheetham, C. R. Acad. Sci. Paris Ser. 2 (1999) 387;
(d) J. Chen, R.H. Jones, S. Natarajan, M.B. Hursthouse, J.M. Thomas, Angew. Chem. Int. Ed. Engl. 33 (1994) 639;
(e) A.R. Cowley, A.M. Chippindale, J. Chem. Soc. Dalton Trans. (1999) 2147;
(f) A. Choudhury, S. Natarajan, C.N.R. Rao, J. Solid State Chem. 155 (2000) 62;
(g) A. Choudhury, S. Neeraj, S. Natarajan, C.N.R. Rao, Angew. Chem. Int. Ed. Engl. 39 (2000) 3091.
[7] (a) M. Cavellec, D. Riou, J.M. Greneche, G. Ferey, Inorg. Chem. 36 (1997) 2181;
(b) K.H. Lii, Y.F. Huang, J. Chem. Soc. Chem. Commun. (1997) 1311;
(c) V. Zima, K.H. Lii, N. Nguyen, A. Ducouret, Chem. Mater. 10 (1998) 1914;
(d) K.H. Lii, Y.F. Huang, J. Chem. Soc., Dalton Trans. (1997) 2221.
[8] (a) J. DeBord, R. Haushalter, J. Zubieta, J. Solid State Chem. (1996) 125;
(b) A.M. Chippindale, F.O.M. Gaslain, A.R. Cowley, A.V. Powell, J. Mater. Chem. 11 (2001) 3172;
(c) Y. Liu, L. Zhang, Z. Shi, H. Yuan, W. Pang, J. Solid State Chem. 158 (2001) 68;
(d) M. Riou-Cavellec, C. Serre, G. Ferey, C. R. Acad. Sci. Paris. t. 2, S. II (1999) 147;
(e) E. Alda, S. Fernandez, J.L. Mesa, J.L. Pizarro, V. Jubera, T. Rojo, Mater. Res. Bull. 37 (2002) 2355;
(f) D. Riou, G. Ferey, J. Solid State Chem. 111 (1994) 422.
[9] (a) N. Guillou, P.M. Foster, Q. Gao, A.K. Cheetham, G. Ferey, Mater. Sci. Forum (2001) 378.
[10] (a) J. Chen, R. Xu, J. Solid State Chem. 80 (1989) 149;
(b) J. Chen, L. Li, G. Yang, R. Xu, J. Chem. Soc. Chem. Commun. (1989) 1217;
(c) A.-H. Liu, S.-L. Wang, Inorg. Chem. 37 (1998) 3415;
(d) M.-Y. Lee, S.-L. Wang, Chem. Mater. 11 (1999) 3588;
(e) S. Ekambaram, S.C. Sevov, Inorg. Chem. 39 (2000) 2405;
(f) Y.-C. Liao, S.-H. Luo, S.-L. Wang, H.-M. Kao, K.-H. Lii, J. Solid State Chem. 155 (2000) 37;
(g) B. Bazan, J.L. Mesa, J.L. Pizarro, L. Lezama, M.I. Arriortua, T. Rojo, Inorg. Chem. 39 (2000) 6056;
(h) B. Bazan, J.L. Mesa, J.L. Pizarro, A. Goñi, L. Lezama, M.I. Arriortua, T. Rojo, Inorg. Chem. 40 (2001) 5691;
(i) B. Bazan, J.L. Mesa, J.L. Pizarro, J.S. Garitaonandia, M.I. Arriortua, T. Rojo, Solid State Sci. 5 (2003) 1291.
[11] J.L. Mesa, A. Goñi, A.L. Brandl, N.O. Moreno, G.E. Barberis, T. Rojo, J. Mater. Chem. 10 (2000) 2779.
[12] A.C.T. North, D.C. Philips, F.S. Mathews, Acta Crystallogr. A 24 (1968) 351.
[13] A. Chandrasekaran, X-RAYACS: Program for Single Crystal X-ray Data Corrections, Chemistry Department, University of Massachusetts, Amherst, USA, 1998.
[14] G.M. Sheldrick, SHELXS 97: Program for the Solution of Crystal Structures, University of Göttingen, Germany, 1997.
[15] G.M. Sheldrick, SHELXL 97: Program for the Refinement of Crystal Structures, University of Göttingen, Germany, 1997.
[16] L.J. Farrugia, J. Appl. Crystallogr. 32 (1999) 837.
[17] T. Hahn, editor, International Tables for X-ray Crystallography, vol. IV, Kynoch Press, Birmingham, England, 1974, p. 99.
[18] E. Dowty, ATOMS, A Computer Program for Displaying Atomic Structures, Shape Software, 521 Hidden Valley Road, Kingsport, TN, 1993.
[19] Powder Diffraction File—Inorganic and Organic, Files No., (a) 21-910; (b) 84-876, Pennsylvania, USA, 1995.
[20] S.-H. Luo, Y.-C. Jiang, S.-L. Wang, H.-M. Kao, K.-H. Lii, Inorg. Chem. 40 (2001) 5381.
[21] H. Arnold, Z. Kristallogr. 177 (1986) 139.
[22] J. Rodriguez-Carvajal, FULLPROF98, Program for Rietveld Pattern Matching Analysis of Powder Patterns, Grenoble, 1998 unpublished.
[23] E.L. Muetterties, L.J. Guggenberger, J. Am. Chem. Soc. 96 (1974) 1748.
[24] (a) B. Bazan, J.L. Mesa, J.L. Pizarro, M.I. Arriortua, T. Rojo, Mater. Res. Bull. 38 (2003) 1193;
(b) K. Nakamoto, Infrared and Raman Spectra of Inorganic and Coordination Compounds, Wiley, New York, 1977.
[25] A.B.P. Lever, Inorganic Electronic Spectroscopy, Elsevier Science Publishers B.V., Amsterdam, 1984.
[26] H.O. Stumpf, L. Ouahab, Y. Pei, P. Bergerat, O. Kahn, J. Am. Chem. Soc. 116 (1994) 3866 and references therein.
[27] (a) H.W. Wijn, L.R. Walker, J.L. Daris, H. Guggenheim, J. Solid State Commun. 11 (1972) 803;
(b) P.M. Richards, M.B. Salamon, Phys. Rev. B 9 (1974) 32;
(c) A. Escuer, R. Vicente, M.A.S. Goher, F. Mautner, Inorg. Chem. 34 (1995) 5707;
(d) A. Bencini, D. Gatteschi, EPR of Exchange Coupled Systems, Springer, Berlin Heidelberg, 1990;
(e) T.T.P. Cheung, Z.G. Soos, R.E. Dietz, F.R. Merrit, Phys. Rev. B 17 (1978) 1266.
[28] R.L. Carlin, Magnetochemistry, Springer, Berlin, Heidelberg, 1986.